Crimson Publishers
Wings to the Research

Research Article

Ge-Doping Impact on the Power Factor of $Sb_{65}Se_{35}$ Nanocrystalline Bulks

Saleh SA[1,2]*

[1]Department, College of Science & Arts, Najran University, KSA

[2]Physics Department, Faculty of Science, Sohag University, Egypt

ISSN: 2576-8840

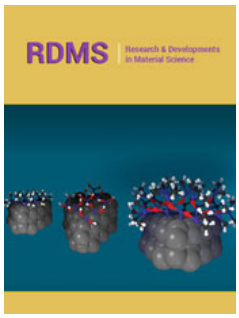

***Corresponding author:** Saleh SA, Department, College of Science & Arts, Najran University, P. O. 1988 Najran, KSA

Submission: February 20, 2025
Published: March 20, 2025

Volume 21 - Issue 3

How to cite this article: Saleh SA. Ge-Doping Impact on the Power Factor of $Sb_{65}Se_{35}$ Nanocrystalline Bulks. Res Dev Material Sci. 21(3). RDMS. 001015. 2025. DOI: 10.31031/RDMS.2025.21.001015

Copyright@ Saleh SA, This article is distributed under the terms of the Creative Commons Attribution 4.0 International License, which permits unrestricted use and redistribution provided that the original author and source are credited.

Abstract

The structure, morphology, transport, and optical properties of Ge-doped antimony selenide alloys prepared by the melt quenching method with the chemical composition $Sb_{65}Se_{35-x}Ge_x$ ($0 \le x \le 20$) were investigated. Structural studies using an X-ray Diffraction (XRD) pattern verified the polycrystalline existence of the synthesized compounds. Field Emission Scanning Electron Microscope (FESEM) images demonstrate the dense microstructure of smaller particles in Ge-doped $Sb_{65}Se_{35}$ compounds. The EDS technique was used to perform quantitative analysis on the undoped and Ge-doped $Sb_{65}Se_{35}$ materials. The Seebeck coefficient, electrical conductivity, and power factor are examined in the ambient temperature range of 100-400K. The findings show that all Ge-substituted materials are n-type thermoelectric components across the entire measurement temperature range. The samples are degenerate semiconductors, according to electrical conductivity measurements. We also computed the power factor for various samples to assess their suitability for thermoelectric applications.

Keywords: Ge-doped $Sb_{65}Se_{35}$; XRD; The electrical conductivity; Seebeck coefficient; Power factor

Introduction

As a result of resource depletion and ecological disasters caused by the use of fossil fuels, researchers are increasingly favoring thermoelectric (TE) materials, which allow for direct thermal-to-electric energy conversion without dangerous liquids, moving parts, or greenhouse emissions.

Even though there has been a substantial improvement in TE performance, the observed conversion efficiency is much lower than the values available in literature. The higher conversion efficiency, on the other hand, generally requires a strong Seebeck coefficient, as well as high electrical conductivity and a low thermal conductivity. Recently, researchers have developed new tactics, such as band structure engineering, multi-scale phonon scattering, and the implementation of resonant levels, to successfully decouple conflicting transport properties and optimize the TE properties of various materials [1-17].

In recent years, researchers have used nanostructures to achieve further declines in lattice conductivity. Even though the goal was to improve the power factor by using quantum confinement effects [5], it looks like phonon scattering on the edges of nano-sized grains was what really made a difference [6,7]. One of the most complicated issues to resolve is how to enhance the electrical conductivity and Seebeck coefficient of inorganic nanoparticles. We can alloy nanostructures with the right elements to improve their electrical conductivity and Seebeck coefficient.

Nanoscale materials may have low thermal conductivity, a high-power factor, improved mechanical characteristics, and greater isotropy [18]. Pulverizing crystallographic nanometric specimens can be a low-cost way of producing the huge volume of material required for

thermoelectric technology to gain widespread use [19].

The present work examines the impact of partial Ge replacement at the Se position on the material properties of Sb-Se, including changes in the microstructure of the material, electronic transitions, and energy band gap. Because Se's valence state in the eutectic Sb-Se is Se^{3+}, adding a quadruple element, Ge^{4+}, can change the environment. This can change the large and small features of the eutectic Sb-Se and give us a better understanding of its TE properties. The rapid implications of this insertion, such as charge compensation impacts and distortion in the crystalline structure of $Sb_{65}Se_{35}$, may lead to the formation of antisite defects (Sb'_{Se} and V'_{Se}), which could significantly impact the electrical and thermoelectric characteristics of the treated $Sb_{65}Se_{35}$ samples. The focus of this research is to determine the influence of Ge doping in $Sb_{65}Se_{35}$, as well as to clarify and interpret the observed behaviors.

Experimental Details

Melting and cold pressing were used to create nanocrystalline $Sb_{65}Se_{35-x}Ge_x$ (x = 0, 5, 10, 15, and 20) bulks. Under vacuum, stoichiometric mixes of high-purity Ge (99%), Sb (99.999%), and Se (99.9999%) granules were packed in graphite-coated tubes and burned to 1123K. After soaking the tubes at 1123K for approximately 5 hours, we quenched them with cold water. The ingots were then crushed into a powder and cold pressed at 5 ton/cm^2 for 3min. A PANalytical X' Pert PRO diffractometer (XRD) and a (JEOL JSM-7600F) FESEM were used to determine the phase structures and microstructure, respectively. The transport properties were measured using pellets with a relative density of 98 percent or higher. A two-probe technique and a temperature gradient method were used to measure electrical conductivity and the Seebeck coefficient, respectively. Using a Perkin Elmer LAMBDA 950 spectrophotometer, reflectance spectroscopy was used to evaluate the band gap of samples. The Archimedes method was used to determine the volume densities (d) of the bulk samples. The electrical properties were all measured perpendicular to the press direction in the current experiments.

Results and Discussion

Microstructure of the synthesized samples

The EDS analysis was used to determine the elemental composition of the fabricated Ge-doped $Sb_{65}Se_{35}$ alloys, and the results are presented in Figure 1. The EDS spectrum revealed several well-defined peaks related to Sb, Se, and Ge, indicating the presence of antimony, selenium, and germanium in the samples. The spectrum showed no other impurity-related peaks, suggesting that the synthesized nanoparticles are Ge-doped $Sb_{65}Se_{35}$. The EDS data shows that each element's estimated average deviation from ideal stoichiometry is less than 1%.

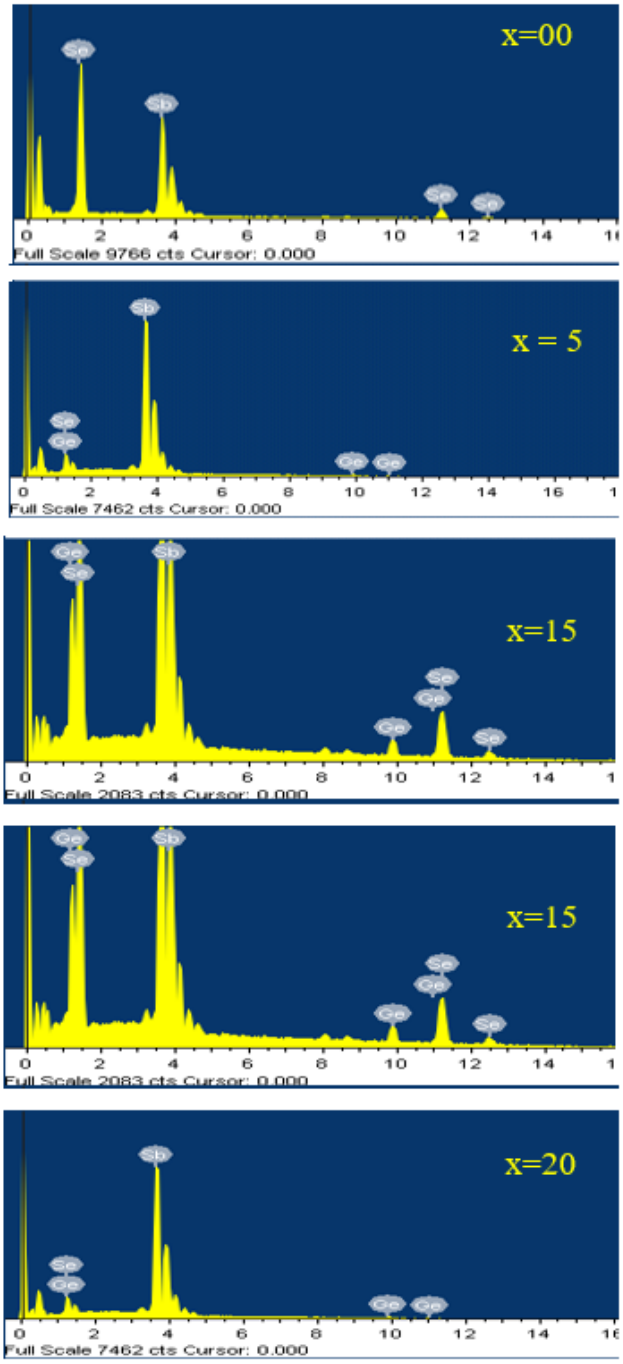

Figure 1: EDS spectra corresponding to the specimens.

Figure 2 illustrates the microstructure of the virgin and Ge-doped compounds produced at five different germanium content levels. The particle was small and exhibited a uniform morphology, as demonstrated. Moreover, FESEM images show well-defined particles with a thin and appreciably fine flake-like structure. Besides this, increasing the concentration of doping tends to reduce the average particle size, signaling that containing high levels of doping is a vital strategy for crystalline refinement. The extremely small particle sizes result in a variety of grain boundaries, which could further improve the thermoelectric properties [20].

Copyright © Saleh SA

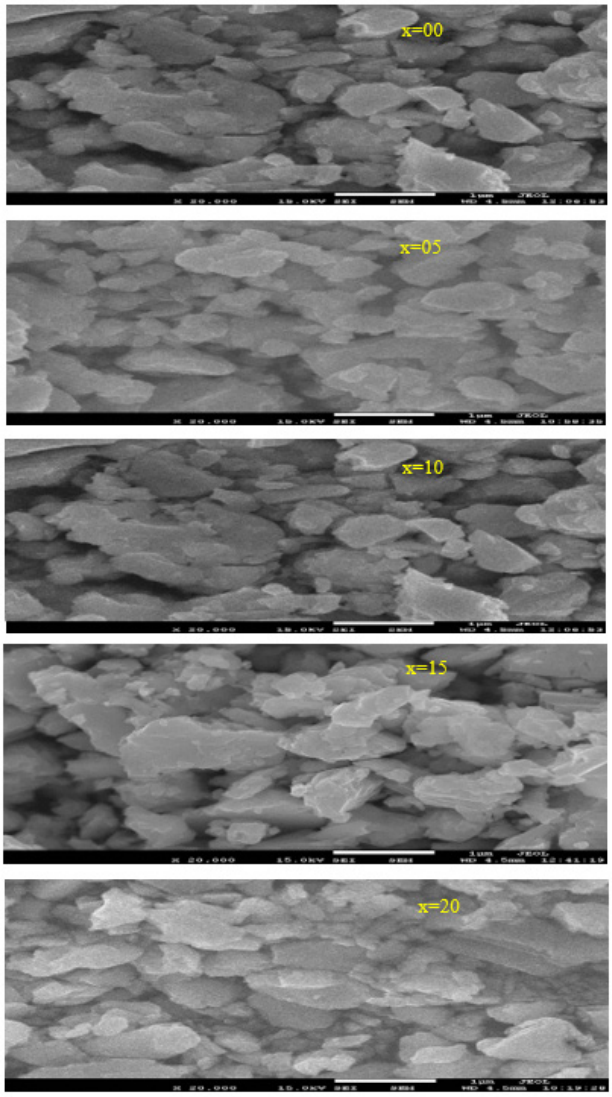

Figure 2: FE-SEM images of Ge-incorporated $Sb_{65}Se_{35}$ ($0 \le x \le 20$) samples.

Figure 3 displays the XRD patterns of pure and Ge-doped samples at room temperature. The observed reflection peaks confirm the single phasic nature of the investigated materials crystallizing in rhombohedral Sb_2Se [21]. The disappearance of secondary phases corresponding to unreacted Ge, Sb, or Se confirms the prepared samples' purity. With the addition of Ge ions, the diffraction peaks shift in the higher-angle direction, revealing that the product tends to accumulate in a comparable but more sophisticated form [22,23]. As the dopant concentration went up, the diffraction peaks got wider and moved toward higher angles. At the same time, some dominant peaks got smaller. This suggests that the rhombohedral structure of Sb_2Se changed without changing the crystal structure. Vegard's law [24] states that the removal of the host atoms substitutes atoms with smaller ionic radii [25]. As the concentration of germanium increases, the strong (200) peak shows a slight red shift and amplitude decreases (except for x = 5), signifying the suppression of crystallization and a decrease in particle size. One used Sherrer's equation to calculate the average crystallite size (C_s) in Table 1 after correcting for instrumental broadening [26]. With different ratios of germanium, particle size decreases. Furthermore, as particle size is reduced, the dislocation density ($\delta = \frac{1}{C_s^2}$) increases. Proposals suggest that a relatively high dislocation density leads to an increase in the band gap of the semiconductor material, as the dislocations significantly isolate from the interatomic distance [21]. As a result, raising the dislocation density makes the materials more resistant to fracture initiation, and high-density high dislocation plays an essential role in strengthening the strength and micro-hardness of the treated materials, as has been proven in earlier work [27].

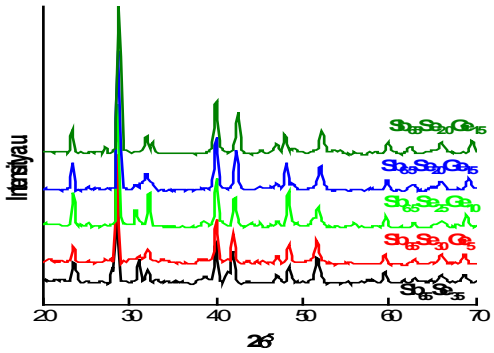

Figure 3: XRD patterns of polycrystalline Ge-doped $Sb_{65}Se_{35}$ ($0 \le x \le 20$) alloys.

Table 1: EDS, XRD and optical band gap results of the synthesized alloys.

Type	Sb	Se	Ge	C_s(nm)	$\delta*10^{11}cm^{-2}$	E_{opt} (eV)
x=00	64.62	35.38	0.00	82.9	12.06	1.18
x=05	64.77	30.27	4.96	90.3	11.07	1.48
x=10	63.98	25.73	10.29	76.2	13.12	0.48
x=15	64.61	19.67	14.72	72.4	13.81	0.64
x=20	63.99	15.30	20.71	62.8	15.92	0.98

Electrical transport and optical properties

Electrical conductivity (σ) is extremely important and required for the applicability of synthesized SSG compounds to TE devices. Figure 4 shows how the electrical conductivity of $Sb_{65}Se_{35}$ bulks changes with temperature from 100K to 400K when different amounts of Ge are added. It is seen that the conductivity decreases monotonically with increasing temperature, which indicates a degenerate semiconductor characteristic. Other works [28-30], possibly due to the distinct Fermi surfaces of the ferromagnetic and paramagnetic states, have reported a similar semiconductor nature.

Copyright © Saleh SA

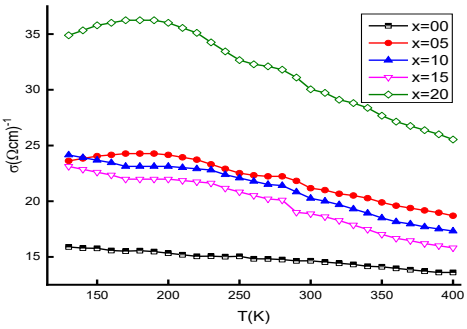

Figure 4: Electrical conductivity (σ) as a function of temperature for various compounds.

The pure sample has the weakest electrical conductivity. The electrical conductivity increases in a non-monotonic manner as the germanium content rises. Moreover, the σ of doped samples is higher than the undoped ones. Electrical conductivity is given by $\sigma = ne\mu$ where n, e and μ are the carrier concentration, the electron charge and the carrier mobility, respectively [31]. This implies that the simultaneous variation of n and μ should influence σ. Moreover, the increase in electrical conductivity when Ge concentration in $Sb_{65}Se_{35}$ samples grows could be due to two factors. In the beginning, when there are more Ge ions in the $Sb_{65}Se_{35}$ lattice, the Ge ions give the lattice freer electrons, which makes it more electrically conductive. It is believed that the Ge ions in the $Sb_{65}Se_{35}$ lattice function as both charge carriers and acceptor impurities. Second, when the concentration of Ge increases, the Ge atoms make more neck contact with Se sites, speeding charge carrier movement and thereby boosting conductivity.

The mobility of carriers (μ) is limited by imperfections such as antisite defects, vacancies, and interface defects, as well as by potential barriers at the grain boundaries that are caused by the smaller particle size [32]. However, chemical bonds can significantly influence carrier mobility. As compared to ionic components, covalent bonds are generally more suitable for carrier transport [33]. The bond polarity contributes to the formation of antisite defects in $Sb_{65}Se_{35}$-based crystals. The more the polarity of the bond between positively and negatively charged atoms decreases, the more likely an antisite defect will form. Despite the fact that antisite defects contain holes and have the ability to counteract electrons, the interaction between vacancies and antisite defects becomes the primary factor, leading to the formation of additional electrons [34]. As a consequence, the carrier concentration rises as the particle size decreases. Furthermore, as particle size decreases, grain boundary, antisite defect, vacancy, and interface defects increase, resulting in greater carrier scattering. Consequently, carrier mobility experiences a limit [35].

The location of the Fermi energy level throughout the component and the type of dispersion process that the charge carriers experience determines the Seebeck coefficient (S) [36]. Then, any alteration of the Fermi level in the substance has the greatest impact on TE power. Furthermore, it is well recognized that S is highly susceptible to the imbalance of the electronic density of states (DOS) at the Fermi level (E_F), with a slight shift in the DOS reflecting a change in its magnitude, which is connected to the charge carrier density (n). The introduction of barriers at interfaces and grain boundaries acts as a filter for low-energy charge carriers [19]. Figure 5 shows S versus temperature for the prepared samples in the measured temperature range. All Ge-doped $Sb_{65}Se_{35}$ samples (x = 0.0-20) showed a negative Seebeck coefficient over the entire temperature range, confirming the dominance of electron-type carriers in thermoelectric transport. The negative values of S across the entire temperature range imply that all of the materials are n-type conductive, with electrons as the predominant charge carrier, as stated previously [37,38]. All samples exhibit a crossover from metallic to semiconducting trend, as indicated by S (T) [39]. In other words, the Ge content x strongly influences the absolute value of the Seebeck coefficient, which first increases and then peaks at a certain point. With the dopant content, the onset of intrinsic conduction (the maxima of the curves) in such samples moves to a different temperature. Moreover, close to the saturation temperature T_{sat}, the magnitude of S reaches its maximum value, after which thermally excited carriers reduce it by increasing the temperature [40]. Excitation across the energy gap forms electron-hole pairs, leading to an increase in bipolar effects as the temperature rises [41]. Thermal excitation causes minority carriers (holes in this case) to emerge as the temperature rises, leading to the creation of the bipolar effect. This presence of electrons and holes is believed to be crucial for S saturation at high temperatures [42]. The bipolar effect, which occurs when the temperature rises and the minority carriers increase, could explain this behavior [43,44,45]. The Goldsmid-Sharp formula can estimate the band gap of the studied samples at a saturation temperature, as it directly correlates the peak of the Seebeck coefficient to the specimen band gap, E_g [46,47]: $E_g = 2e|S|_{max} T_{sat}$, where e represents the elementary charge, $|S|_{max}$ is the maximum Seebeck coefficient for the bipolar effect sample, and T_{sat} signifies the absolute temperature at which S_{max} appears. E_g values for various samples (x = 0, 5, 10, 15, and 20) are roughly 0.0119, 0.0091, 0.0081, 0.0092, and 0.0076eV, respectively. To put it differently, the smaller the particle size, the greater the band gaps, and hence the higher the intrinsic excitation temperature.

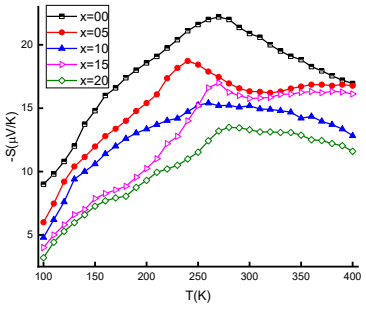

Figure 5: Seebeck coefficient versus temperature for all compositions.

Copyright © Saleh SA

The Seebeck coefficient changes when Ge is added, which can be linked to changes in the concentration of carriers as [48]: $S = \frac{8\pi^2 k_B^2}{3eh^2} \times T\left(\frac{\pi}{3n}\right)^2$,where h is the Planck constant and k_B is the Boltzmann constant. A drop in the Seebeck coefficient causes the concentration of carriers to rise. It signifies that a lower value of S corresponds to a larger carrier concentration (n).

The $Sb_{65}Se_{35}$-based alloys' carrier concentration, on the other hand, is vulnerable to lattice imperfections caused by mechanical deformation. Therefore, the deformation-induced donor-like effect, which introduces an excess of negative carriers in the lattice, is responsible for the simultaneous increase in S. As a consequence, the new point defects introduced into the lattice as a result of the plastic deformation will alter the material's transport behavior, as previously stated [49,50]. The combination of antisite defects and vacancies creates a donor-like effect during the grinding and heat treatment process, which can lead to an increase in electron production [51]. More mechanical stress accumulates as the particle size of crystals decreases, resulting in more antisite defects and vacancies. Antisite defects are simpler to arise when the difference in electronegativity between the components that make up the thermoelectric material is minimal [52]. An increase in the size mismatch between the cation and anion atoms promotes the creation of anion vacancies [53].

Nevertheless, it is worthwhile noting that the samples with germanium content exhibit relatively lower Seebeck coefficients owing to an increase in carrier concentration [54]. Moreover, thermally induced boundary resistance between particles, resulting in a thermal gradient over the interfaces, can diminish the Seebeck coefficient in nanostructured materials, or electron-filtering processes at the connections can increase it [55].

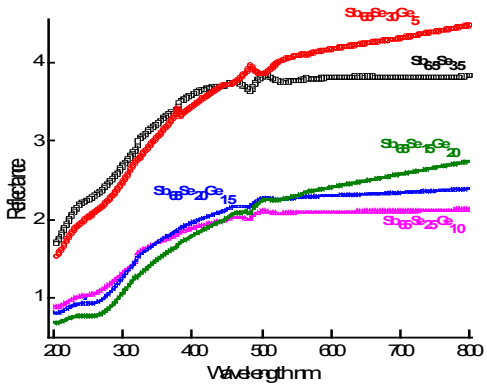

Figure 6: Wavelength dependence of the reflectance for all compositions.

Finally, optical properties serve only as a tool to gain insight into the contributions of the electronic band structure, which in turn shape the electronic transport properties. Understanding the nature of the band structure has paved the way for future band engineering research involving the proper alloying of the system, which could result in significant TE performance enhancements. To study the effect of Ge substitution on the band gap of $Sb_{65}Se_{35}$, Diffuse Reflectance Spectroscopy (DRS) was performed on the specimens at 300K. Figure 6 shows the UV–vis reflectance of all samples as a function of wavelength at room temperature. Raising the wavelengths significantly increased the diffused reflectance of both pure and doped samples. In addition, the incorporation of Ge dopant into the host $Sb_{65}Se_{35}$ reduces diffused reflectance. Pure, 5, 10, 15, and 20 Ge-doped $Sb_{65}Se_{35}$ have absorption edges that begin at 394, 404, 413, 380, and 369nm, respectively. Doping causes a change in the absorption edge, which implies a change in the band structure.

The indirect band gap of undoped and doped samples is plotted against photon energy (hν). One extracted the band gap values, as shown in Figure 7, by graphing the root square of the Kubelka-Munk (KM) function [56] versus hν and then projecting the linear section of the $[F(R)h\nu]^{0.5}$ plot to the energy axis. Table 1 states that an increase in Ge doping causes the E_{opt} to rise from 0.48 to 1.48eV. The rising trend in E_{opt} would result in fewer carriers and a lower carrier density, revealing an increase in the materials' resistance. Ge-dopants will change E_{opt} and thus acquire resistance as a result of this observation and hypothesis [57].

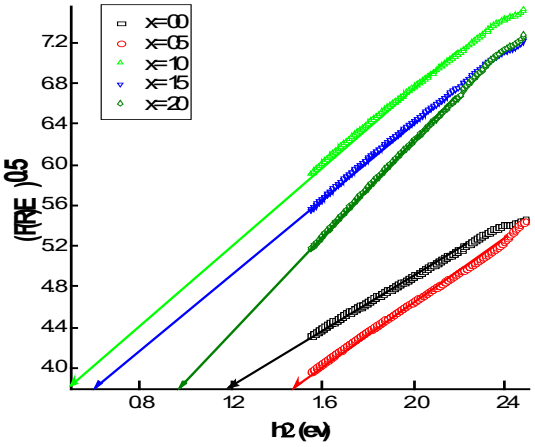

Figure 7: Variation of the absorption coefficient with energy in various alloys.

The Power Factor (PF) of $Sb_{65}Se_{35}$ doped with Ge, which must have an average value (W $m^{-1}K^{-2}$) of approximately 10^{-3} for materials used in contemporary devices [58], characterizes the electrical performance of TE materials. We computed the Power Factor (PF) across the entire temperature range of the data to determine the effectiveness of using these compositions as TE generators. Figure 8 shows the temperature dependence of the PF plots. Clearly, as the temperature increases, the PF rises and then declines, reaching maxima at specific temperatures that depend on the Ge content. The power factor of $Sb_{65}Ge_5Se_{30}$ is 0.8 (mW m^{-1} K^{-2}) at 240K, which is significantly lower than that of state-of-the-art TE alloys.

Copyright © Saleh SA

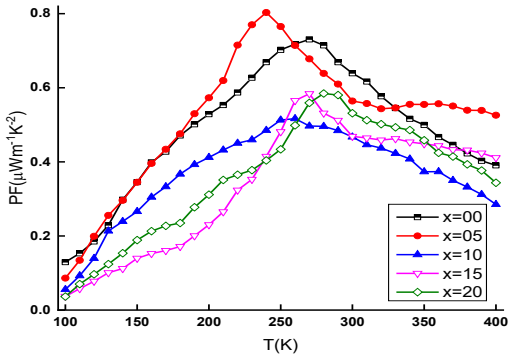

Figure 8: Temperature dependence of the power factor for all compositions.

These results show that $Sb_{65}Se_{35}$ is a good thermoelectric material that needs more attention. There are many ways to improve $Sb_{65}Se_{35}$'s power factor, such as alloying, nano structuring, and band modification, which could make PF even better. Moreover, the high performance of $Sb_{65}Se_{35}$ implies the discovery of new thermoelectric materials in systems with similar complex band structures.

Conclusion

Polycrystalline $Sb_{65}Se_{35}$ doped with Ge materials were synthesized by melt quenching method. There were no secondary phases detected in the pure rhombohedral Sb_2Se phase. All of the crystals exhibit microstructures of various shapes and sizes. The temperature dependence of electrical conductivity measurements shows that all compositions have metallic-like behavior. Electrons are the predominant charge carriers, according to Seebeck coefficient measurements. The Ge content significantly influences the electrical and TE properties of the system under investigation. For the $Sb_{65}Ge_5Se_{30}$ composition, the highest power factor value was 0.8 (mW m^{-1} K^{-2}) observed at T = 240K. All of these characteristics are critical in determining a material's suitability for use in thermoelectric devices. Furthermore, the high performance of $Sb_{65}Se_{35}$ suggests the possibility of developing new thermoelectric materials with similar complex band structures.

Declaration of competing interest

The authors declare that they have no known competing financial interests or personal relationships that could have appeared to influence the work reported in this paper.

References

1. Thomas R, Ashok Rao, Zhao-Ze Jiang, Yung-Kang Kuo (2021) Effects of Bi doping on the electrical and thermal transport properties of Cu_2SnSe_3. Mater Sci Semicond Processing 134: 106032.
2. Bourges C, Rabih Al, Yuzuru Miyazaki (2020) Off-stoichiometry effect on thermoelectric properties of the new p-type sulfides compounds Cu_2CoGeS_4. J Alloys Compd 826: 154240.
3. Fu C, Zhu T, Liu Y, Xie H, Zhao X (2015) Band engineering of high-performance p-type FeNbSb based half-Heusler thermoelectric materials for figure of merit zT > 1. Energy Environ Sci 8: 216-220.
4. Tan X, Wang H, Liu G, Noudem JG, Hu H, et al. (2018) Designing band engineering for thermoelectrics starting from the periodic table of elements. Materials Today Physics 7: 35-44.
5. Zhao LD, Lo SH, He J, Li H, Biswas K, et al. (2011) High performance thermoelectrics from earth-abundant materials: Enhanced figure of merit in pbs by second phase nanostructures. J Am Chem Soc 133: 20476-20487.
6. Johnsen S, He J, Androulakis J, Dravid VP, Todorov I, et al. (2011) Nanostructures boost the thermoelectric performance of PbS. J Am Chem Soc 133: 3460-3470.
7. Kim W, Zide J, Gossard A, Klenov D, Stemmer S, et al. (2006) Thermal conductivity reduction and thermoelectric figure of merit increase by embedding nanoparticles in crystalline semiconductors. Phys Rev Lett 96: 045901.
8. Jabar B, Qin X, Mansoor A, Ming H, Huang L, et al. (2020) Enhanced thermoelectric performance of n-type $Sn_xBi_2Te_{2.7}Se_{0.3}$ based composites embedded with in-situ formed SnBi and Te nano inclusions. Composites Part B 197: 108151.
9. Symeou E, Karyou M, Delimitis A, Constantinou M, Constantinides G, et al. (2022) Preparation of highly efficient thermoelectric Bi-doped $Mg_2Si_{0.55-x}Sn_{0.4}Ge_x$ (x = 0 and 0.05) materials with a scalable mechanical alloying method. J Phys Chem Solids 161: 110472.
10. Fu C (2016) Adv Sci 3: 1600035.
11. Poudel B, Hao Q, Ma Y, Lan Y, Minnich A, et al. (2008) High-Thermoelectric Performance of Nanostructured Bismuth Antimony Telluride Bulk Alloys. Science 320: 634-638.
12. Takagiwa Y, Isoda Y, Goto M, Shinohara Y (2018) Conduction type control and power factor enhancement of the thermoelectric material $Al_2Fe_3Si_3$. J Phys Chem Solids 118: 95-98.
13. Heremans JP, Wiendlocha B, Chamoire AM (2012) Resonant levels in bulk thermoelectric semiconductors. Energy Environ Sci 5: 5510-5530.
14. Zhang Q (2021) Energy Environ Sci 5: 5246-5251.
15. Zhang Q (2013) Proc Natl Acad Sci USA 110: 13261-13266.
16. Lv T, Li Z, Liu Y, He J, Zhou D, et al. (2019) Improving thermoelectric performance of $(Bi_{0.2}Sb_{0.8})_2(Te_{0.97}Se_{0.03})_3$ via Sm-doping. J Alloys Compd 787: 909-917.
17. Tan G, Zeier WG, Shi F, Wang P, Snyder GJ, et al. (2015) High thermoelectric performance SnTe-In_2Te_3 solid solutions enabled by resonant levels and strong vacancy phonon scattering. Chem Mater 27: 7801-7811.
18. Kanatzidis MG, Chung DY, Sootsman JR (2009) New and old concepts in thermoelectric materials. Angew Chem Int Ed 48: 8616 - 8639.
19. Dresselhaus MS, Chen G, Tang MY, Yang RG, Lee H, et al. (2007) New Directions for low-dimensional thermoelectric materials. Adv Mater 19(8): 1043-1053.
20. Ni HL, Zhu TJ, Zhao XB (2005) Thermoelectric properties of hydrothermally synthesized and hot pressed n-type Bi_2Te_3 alloys with different contents of Te. Mater Sci Eng B 117(2): 119-122.
21. Saleh SA (2011) Synthesis and characterization of $Sb_{65}Se_{35-x}Ge_x$ alloys. Mate Sci Appl 2: 950-956.
22. Matsunaga T, Yamada N (2004) Jpn J Appl Phys 43: 4704.
23. Prokhorov E, Mendoza-Galván A, González-Hernández J, Chao B (2007) Effects of Ge addition on the optical and electrical properties of eutectic $Sb_{70}Te_{30}$ films. J Non-Cryst Solids 353: 1870-1874.
24. Denton AR, Ashcroft NW (1991) Phys Rev A: At Mol Opt Phys 43: 3161-3164.
25. González-Hernández J (1992) Appl Phys Comm 11: 557.
26. Subramanian S, Padiyan DP (2008) Effect of structural, electrical and optical properties of electrodeposited bismuth selenide thin films in polyaniline aqueous medium. Mater Chem Phys 107: 392-398.
27. Wang J, Lu Y, Zhou D, Sun L, Xie L, et al. (2019) Mechanical properties and microstructural response of 2A14 aluminum alloy subjected to multiple laser shock peening impacts. Vacuum 165: 193-198.

Copyright © Saleh SA

28. Hsu KF (2004) Science 303: 818.
29. Ibrahim MM, Saleh SA, Abdel Hakeem AM (2007) Studies on sintering effect on the transport properties of $Pb_{1-x}Sm_xSe$. Phys Scrip 75: 660-665.
30. Figiel H, Budziak A, Żukrowski J, Wiesinger G, Ouladdiaf B (2004) Neutron diffraction studies of $TbMn_2D_x$ and $ErMn_2D_2$. J Mag Mag Mater 272-276: 585-586.
31. Lv T, Li Z, Liu Y, He J, Zhou D, et al. (2019) Improving thermoelectric performance of $(Bi_{0.2}Sb_{0.8})_2(Te_{0.97}Se_{0.03})_3$ via Sm-doping. J Alloys Compd 787: 909-917.
32. Kuo CH, Jeng MS, Ku JR, Wu SK, Chou YW, et al. (2009) p-Type PbTe thermoelectric bulk materials with nanograins fabricated by attrition milling and spark plasma sintering. J Elect Mat 38: 1956-1961.
33. Shi W, Wu F, Wang K, Yang J, Song H, et al. (2014) Preparation and thermoelectric properties of yttrium-doped Bi_2Te_3 flower-like nano powders. J Elect Mater 43: 3162-3168.
34. Son JH, Oh MW, Kim BS, Park SD, Min BK, et al. (2013) Effect of ball milling time on the thermoelectric properties of p-type $(Bi,Sb)_2Te_3$. J Alloy Compd 566: 168-174.
35. Zhang C (2017) Adv Eng Mate 19: 1600696.
36. Yadav AA (2012) Synthesis and characterization of Fe doped cadmium selenide thin films by spray pyrolysis. J Alloys Compd 543: 129-134.
37. Bhattacharya RN, Pramanik P (1982) A photoelectrochemical cell based on chemically deposited Sb_2Se_3 thin film electrode and dependence of deposition on various parameters. Solar Energy Mater 6: 317.
38. Garcia VM, Nair MTS, Nair PK, Zingaro RA (1997) Chemical deposition of bismuth selenide thin films using N,N-dimethylselenourea. Semicond Sci Technol 12(5): 645.
39. Rocksted HK, Flasck R, Iwasa S (1972) Seebeck coefficient in amorphous chalcogenide films. J Non-Cryst Solids 8-10: 326.
40. Ibrahim MM, Saleh SA, Ibrahim EMM, Abdel Hakeem AM (2008) Electrical and thermoelectric properties of PbSe doped with Sm. J Alloys Compd 452: 200.
41. Goldsmid HJ (2010) Introduction to thermoelectricity.
42. Wang S (2012) J Mater Chem 22: 20943-20951.
43. Hong M (2016) Nanoscale 8: 8681-8686.
44. Yang J (2015) Thermoelectrical properties of lutetium-doped Bi_2Te_3 bulk samples prepared from flower-like nano powders. J Alloys Compd 619: 401-405.
45. Yaprintsev M, Vasil'ev A, Ivanov O (2020) Thermoelectric properties of the textured $Bi_{1.9}Gd_{0.1}Te_3$ compounds spark-plasma-sintered at various temperatures. J European Ceramic Society 40: 742-750.
46. Goldsmid HJ, Sharp JW (1999) Estimation of the thermal band gap of a semiconductor from seebeck measurements. J Elec Mater 28: 869-872.
47. Gibbs ZM (2015) Appl Phys Lett 106: 022112.
48. Liu B (2018) Thermoelectric properties of In-substituted Ge-based clathrates prepared by HPHT. J Materiomics 4: 68-74.
49. Zhang Z, Sharma PA, Lavernia EJ, Yang N (2011) Thermoelectric and transport properties of nanostructured Bi^2Te^3 by spark plasma sintering. J Mater Res 26: 475-484.
50. Zhao L, Zhang BP, Liu WS, Zhang HL, Li JF, et al. (2009) Effects of annealing on electrical properties of n-type Bi_2Te_3 fabricated by mechanical alloying and spark plasma sintering. J Alloys Compd 467: 91-97.
51. Navratil J, Starý Z, Plecháček T (1996) Thermoelectric properties of p-type antimony bismuth telluride alloys prepared by cold pressing. Mater Res Bull 31(12): 1559.
52. Stary Z, Horák J, Stordeur M, Stölzer M (1988) Antisite defects in $Sb_{2-x}Bi_xTe_3$ mixed crystals. J Phys Chem Solids 49: 29-34.
53. Horak J, Stary Z, Lošťák P, Pancíř J (1990) Anti-site defects in n-Bi_2Se_3 crystals. J Phys Chem Solids 51: 1353-1360.
54. Hu X, Xiang Q, Kong D, Fan X, Feng B, et al. (2019) The effect of Ni/Sn doping on the thermoelectric properties of BiSbTe polycrystalline bulks. J Solid State Chemistry 277: 175-181.
55. Zide JMO (2006) Phys Rev B 74: 205335.
56. Araújo TR, Medeiros R, Oliveira AAS, Nascimento RBA, Maziviero FV, et al. (2021) Optical, morphological, physical and crystalline properties of type structures $Ce_xAl_{2-x}O_3$ (x = 0; 0.25; 0.50; 0.75 and 1) obtained by microwave assisted combustion. Materials Science in Semiconductor Processing 134: 106014.
57. Zou H, Zhu X, Hu Y, Sui Y, Zhang J, et al. (2017) Improving the thermal stability and phase change speed in $Sb_{70}Se_{30}$ films through Er doping. J Mater Sci: Mater Electron 28: 17719-17725.
58. Fujikane M, Kurosaki K, Muta H, Yamanaka S (2005) Thermoelectric properties of Ag_8GeTe_6. J Alloys Compd 396(1-2): 280-282.

Copyright © Saleh SA